ELSEVIER

International Journal of Mass Spectrometry 181 (1998) 31–41

International Journal of Mass Spectrometry

Laboratory investigations of negative ion molecule reactions of formic and acetic acids: implications for atmospheric measurements by ion-molecule reaction mass spectrometry

Jyrki Viidanoja[1,*], Thomas Reiner[2], Frank Arnold

Abteilung Atmosphärenphysik, Max-Planck-Institut für Kernphysik, Postfach 103980, D-69029, Heidelberg, Germany

Received 31 July 1998; accepted 17 August 1998

Abstract

Laboratory measurements of gas-phase ion-molecule reactions of several negative ion species with formic and acetic acid have been carried out. A flow reactor operating at a temperature of 293 ± 3 K and total gas pressures of either 3 or 9 hPa was used. The negative reagent ion species investigated included OH^-, O_2^-, O_3^-, CO_4^-, CO_3^-, $CO_3^-H_2O$, $HCO_3^-H_2O$, NO_3^-, $NO_3^-H_2O$, NO_2^-, and $NO_2^-H_2O$. The reactions were found to proceed either via proton transfer or clustering. Our measurements of ion-molecule reactions of negative ions with gaseous formic and acetic acids provide a firm base for quantitative detection of these acidic trace gases in the atmosphere by negative ion ion-molecule reaction mass spectrometry. (Int J Mass Spectrom 181 (1998) 31–41) © 1998 Elsevier Science B.V.

Keywords: Formic acid; Acetic acid; Chemical ionisation; Tropospheric chemistry

1. Introduction

Organic acids are important atmospheric trace gases as they contribute significantly to the acidity of atmospheric condensed water and acid precipitation. Thereby organic acids also have an influence on chemical processes in cloud droplets as, e.g. liquid phase oxidation of SO_2 by H_2O_2 which depends critically on the pH value of cloud droplets.

Sources of atmospheric organic acids include both natural and manmade, as well as direct and indirect ones. Direct sources include emissions from the biosphere, biomass burning, and motor vehicle exhaust [1–3]. Secondary sources include photochemical oxidation of atmospheric hydrocarbons [3–6]. Formic and acetic acids are both formed via reactions of biogenic and anthropogenic alkenes with ozone [7, 8], while acetic acid can also be formed by reactions of peroxy acetyl radicals ($CH_3C(O)O_2$) with HO_2 and organic peroxy radicals, particularly CH_3O_2 [5, 9–11].

Gaseous formic and acetic acids (HCOOH, CH_3COOH) have previously been measured in the atmosphere mostly by filter, mist chamber, and denuder methods [12]. In addition, aircraft-based ion-molecule reaction mass spectrometry (IMRMS) in-

* Corresponding author.

[1]Permanent address: Department of Physics, P.O. Box 9, FIN-00014, University of Helsinki, Finland.

[2]Present address: Abteilung Biogeochemie, Max-Planck-Institut für Chemie, Postfach 3060, D-55020 Mainz, Germany.

PII S1387-3806(98)14151-9

struments also have found signatures of formic and acetic acid. Chapman et al. [13] used the product ions $HCOO^-$ and CH_3COO^- resulting from the reactions of unspecified negative ions with gaseous formic and acetic acid to determine these acidic trace gases. Therefore, his approach involved only an empirical calibration whereas systematic laboratory measurements of the requisite ion-molecule reactions were lacking. Our group at MPIK, Heidelberg in their aircraft-based IMRMS experiments also found signatures of negative product ions resulting from ion-molecule reactions of formic and acetic acid. These signature included $HCCO^-$, CH_3COO^-, NO_3^-HCOOH, and $CO_3^-CH_3COOH$.

From previous atmospheric measurements it was found that formic and acetic acid are usually the most abundant organic acids in the atmosphere [14] and that their atmospheric volume mixing ratios typically range between a few hundred parts per trillion (pptv) to 10 parts per billion (ppbv) in some instances [15, 16]. They are often present in atmospheric condensed water due to their substantial solubility in water. They contribute significantly to the acidity of cloud water and precipitation in both remote and urban areas [17, 18]. Indeed wet and dry deposition are major sinks of these acidic trace gases.

The present article reports on laboratory measurements of gas-phase reactions of negative ions with formic and acetic acids. These measurements provide a firm base for the detection of these acidic trace gases by our IMRMS method.

2. Experimental

The present laboratory experiments were performed using a flow tube ion reactor with a quadrupole mass spectrometer for ion analysis and detection. The flow reactor consisted of a stainless steel flow tube (4 cm i.d.) with an ion source and inlet ports for the addition of reactant gases and water vapour. A similar experimental setup has been used for previous investigations of ion-molecule reactions at our laboratory and is described in detail elsewhere [19, 20].

The experiments were performed in a laminar, mixed N_2 and O_2 (close to atmospheric composition), gas flow of 10 standard liters per minute at standard temperature and pressure (slm). At a flow reactor pressure of 3 hPa the bulk flow velocity was about 50 m/s. The reactant ions O_2^- and O_3^- were produced by a capillary tube ion source (CIS) within 1–2 slm O_2 source gas flow. A detailed description of the ion source and of the reactant ion evolution has been given previously [19]. For the generation of the reactant ions CO_3^- and CO_4^- or NO_3^- and NO_2^- small amounts of CO_2 or NO_2 were introduced into the source gas flow. In addition to the more abundant ions, the ion source also produced less abundant ions, particularly OH^- and HCO_3^-. Hydrated reactant ions $X^-(H_2O)_n$ were produced by introducing water vapour into the flow reactor, from a water reservoir located 15 cm upstream of the ion source.

Known fluxes of formic and acetic acids were generated by a permeation source (Kin-Tek Laboratories). Acid vapour diffusing from the permeation source was diluted with a nitrogen gas flow of 1.1 slm, which was passed through the permeation source at atmospheric pressure. The acids were added to the flow reactor 46.5 cm downstream of the ion source through a teflon tube inlet with a critical orifice. The flow through the critical orifice fabricated from stainless steel was 0.77 slm. The remainder of the 1.1 slm permeation source flow was discarded. Acid concentrations in the flow reactor were calculated from the gas flows, the flow reactor pressure, and the known emission rates of the permeation tubes.

The distance between the acid inlet and the ion source was long enough for the reactant ion evolution being completed before the ions entered the reaction zone. This was experimentally verified by observing the ion composition for different distances between the ion source and the mass spectrometer. The reaction zone between the acid inlet and the mass spectrometer had a total length of 97.5 cm.

For most measurements the concentrations of the acids were changed by varying the temperature of the permeation source in steps of 5 or 10 K and by allowing the source to stabilise thermally for about 30 min. In some experiments acid concentrations were varied by varying the nitrogen flow through the

permeation source (dilution flow) and keeping the temperature constant. Both methods gave essentially identical results.

The mass discrimination of the quadrupole instrument was determined from integral spectra and by fitting the product ion yields to equal the amount of reacted reactant ions for those reactions, which produced only one distinct product ion species. The residence time t_R of the ions between the acid inlet and the quadrupole mass spectrometer was measured by pulsing the ion swarm with a repeller grid. For the 3 and 9 hPa measurements residence times of 10.5 ± 0.5 and 32 ± 1 ms, respectively, were measured. A ratio of 0.58 for the bulk gas velocity and the ion velocity was measured, in good agreement with expectations from laminar diffusion theory. Mixing times of the acids with the buffer gas of 0.5 ± 0.5 ms at 3 hPa and 1.0 ± 1.0 ms at 9 hPa were estimated by making measurements with different acid inlet positions.

In the presence of water vapour in the flow reactor a rapid ion hydration equilibrium was established. The ion hydration equilibrium was also maintained when reactant acid was added, even in those cases where the reactivities of the different hydrates with the acid were different. The existence of this permanent hydration equilibrium was experimentally verified by the observation that, even though the absolute abundance of the reactant ions decreased, the relative abundance of the different hydrates did not vary significantly with acid concentration. Since in most cases several ion hydrates existed simultaneously, an effective reaction rate coefficient, k_{eff}, being a weighted sum of the individual reaction rate coefficients k_i of the individual hydrates, was measured

$$k_{\text{eff}} = \sum_i x_i k_i;\ \sum_i x_i = 1 \qquad (1)$$

The weighting factors (x_i) are equal to the relative abundance of each hydrate $X^-(H_2O)_i$. If the rate coefficient of the bare reactant ion k_0 is known the rate coefficients of the hydrated ions ($i > 0$) can be calculated from Eq. (1).

Carboxylic acids are known for their ability to dimerize efficiently both in the gas and liquid phases [21, 22]. This can cause problems in the determination of reaction rate coefficients and reaction channels for monomers if dimer concentrations are significant. Equilibrium constants of dimer formation and dissociation for formic and acetic acids are given in the literature. Using the values of Taylor and Bruton [21] and Buttner and Maurer [22] we calculate that under the present experimental conditions less than 5% of formic acid and less than 30% of acetic acid were in the dimer form in the permeation source flow (at atmospheric pressure). When the acid entered the low pressure flow reactor, it was diluted and rapidly attained a new equilibrium with respect to dimerisation [23, 24]. Under the conditions in the flow reactor less than 0.001% and 0.05% of formic and acetic acid molecules, respectively, were in the dimer forms if the equilibrium constants are assumed to be pressure independent.

3. Results

3.1. Formic acid reactions

Fig. 1 shows the CO_3^- and NO_3^- reactant ions and their product ions as function of the HCOOH concentration in the flow reactor. A flow reactor pressure of 3 hPa nitrogen and a constant reaction time of t_R = 10.5 ms were used in both experiments. The reagent ion CO_3^- [Fig. 1(a)] reacted with HCOOH in a proton exchange reaction producing the $HCOO^-$ ion. Secondary reactions of $HCOO^-$ with HCOOH produced the higher order cluster ions $HCOO^-(HCOOH)_{1,2}$ [Fig. 1(a)]. In contrast to CO_3^-, the reaction of NO_3^- [Fig. 1(b)] with HCOOH proceeded solely by a three body addition reaction leading to the NO_3^-HCOOH cluster ion. This is evident since the proton affinity of NO_3^- is much lower than that of $HCOO^-$ (Table 1). Therefore no proton transfer from HCOOH to NO_3^- can occur. The same argument is true for NO_2^-, where the only product observed was the cluster ion NO_2^-HCOOH. Secondary reactions of NO_3^-HCOOH producing the higher order cluster ion $NO_3^-(HCOOH)_2$ were also observed. Reactions of O_3^- and OH^- with HCOOH produced $HCOO^-$ ions.

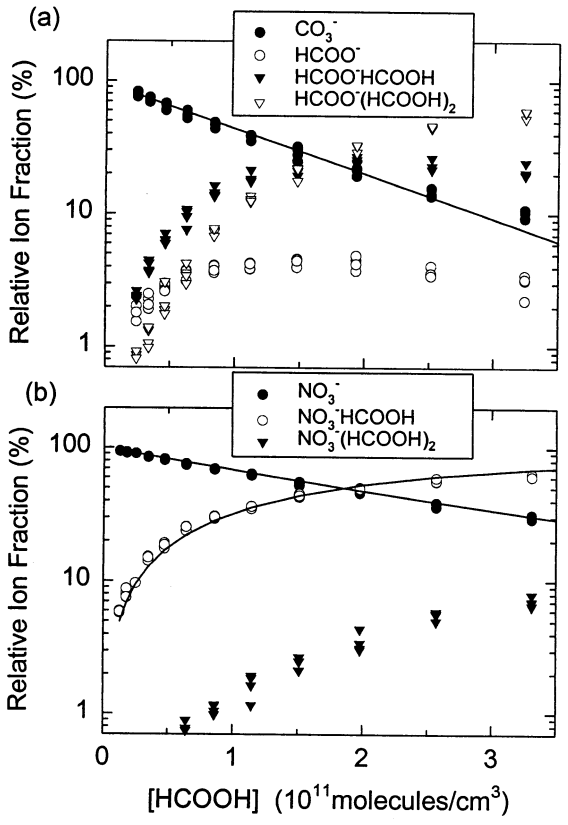

Fig. 1. Reactant and product ions vs the concentration of formic acid for the reactions of formic acid with (a) CO_3^- and (b) NO_3^-.

In the presence of water vapour, reactions were observed for the hydrated ions similar to those of the bare ions. The $HCOO^-$ product ions exhibited a strong tendency for hydration. Equilibrium constants of hydratation of $HCOO^-(H_2O)_n$ were estimated to be 3.5×10^5, 8×10^4, and 6×10^3 atm^{-1} for n = 0, 1, and 2, respectively, at 293 ± 3 K.

Table 1
Proton affinities (PA) of selected anions [25]

Anion	PA (X^-) (kJ mol^{-1})
OH^-	1635
O_2^-	1476
CH_3COO^-	1459
$HCOO^-$	1445
NO_2^-	1421
NO_3^-	1358

The reactions of HCOOH with O_2^- and CO_4^- proceeded by a three-body association and a two-body exchange reaction, respectively, yielding the common cluster ion product O_2^-HCOOH, which further reacted with HCOOH producing the second $O_2^-(HCOOH)_2$ cluster ion. It is possible that CO_4^- and O_2^- reactant ions and/or their O_2^- cluster ion products may also react by proton transfer reactions producing the same product ion ($HCOO^-$) as CO_3^- and O_3^-. The proton affinity of O_2^- is higher than that of $HCOO^-$ or CH_3COO^- (Table 1), which makes the proton transfer reaction at least thermodynamically feasible. However, the product ions of this possible second reaction channel of CO_4^- and O_2^- could not be discerned from the product ions of the much more abundant CO_3^- or O_3^- reactant ions in the same experiments.

3.2. Acetic acid reactions

The behaviour of the CO_3^- ion and its reaction products with varying acetic acid concentration in the flow reactor is shown in Fig. 2(a). The reagent ion CO_3^- decreases with increasing CH_3COOH concentration and the products are CH_3COO^- and $CO_3^-CH_3COOH$ cluster ions. Further reactions of CH_3COO^- and $CO_3^-CH_3COOH$ with CH_3COOH produce higher cluster ions of the form $CH_3COO^-(CH_3COOH)_n$ and $CO_3^-(CH_3COOH)_n$. Cluster ions with n up to 2 were observed. Similar to $HCOO^-$ the hydration tendency of CH_3COO^- is high. Ionic clusters of the mixed type $CO_3^-CH_3COOH \cdot H_2O$ and $CH_3COO^-CH_3COOH \cdot H_2O$, were also observed, with $CH_3COO^-CH_3COOH$ showing a much stronger tendency for hydration than $CO_3^-CH_3COOH$.

In contrast to CO_3^- the NO_3^- ion does not react with CH_3COOH in a proton exchange reaction. It only forms the association product $NO_3^-CH_3COOH$ [Fig. 2(b)]. This is expected since the proton affinity of CH_3COO^- is much larger than that of NO_3^-. The same argument is true for NO_2^-. The $NO_3^-CH_3COOH$ cluster ions were also found to produce further clusters with CH_3COOH. However, the second cluster $NO_3^-(CH_3COOH)_2$ was much less abundant than the

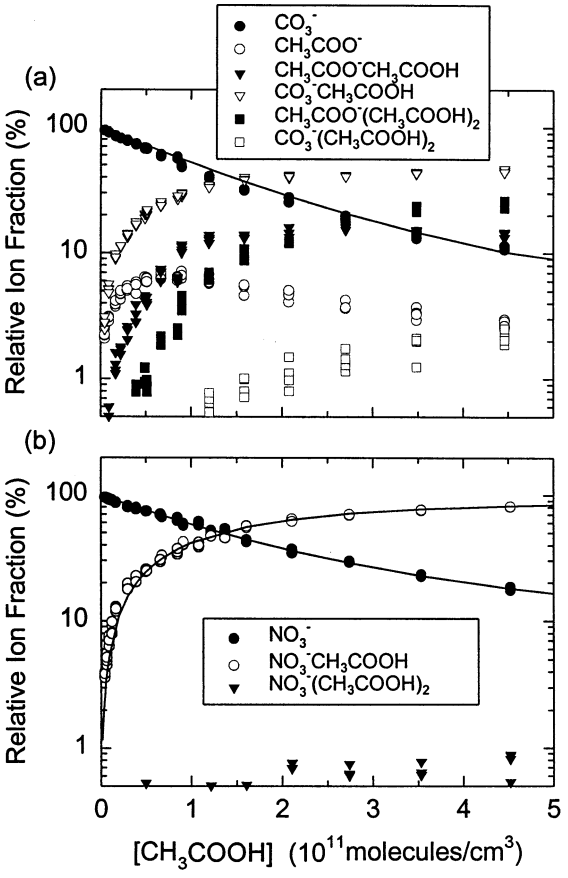

Fig. 2. Reactant and product ions vs the concentration of acetic acid for the reactions of acetic acid with (a) CO_3^- and (b) NO_3^-.

second CH_3COOH cluster of CO_3^- or CH_3COO^-. Similar reactions as in the case of the bare ions were observed if water was added. Reactions of CO_4^- and $O_2^-(H_2O)_{1,2,3,4}$ were also observed, producing the $O_2^-CH_3COOH$ cluster ion.

4. Discussion

The decay curves of proton transfer reactions, as, e.g. CO_3^- + HCOOH [Fig. 1(a)], all showed the expected exponential behaviour. By contrast some of the reactions producing cluster ions, like NO_3^-HCOOH, $CO_3^-CH_3COOH$ or $NO_3^-CH_3COOH$, exhibited deviations from the expected exponential behaviour. In the case of formic acid several reactions not producing cluster products showed the expected exponential decrease of the reactant ions with increasing HCOOH concentration, indicating nominal operation of the permeation sources. In these cases the reaction rate coefficients were determined from the linear decrease of the logarithm of the count rate with increasing formic acid concentration. The reaction rate coefficients for the formic acid reactions are given in Table 2.

In the case of acetic acid all reactions studied produced cluster products to some extent. In this case the nominal operation of the permeation sources was checked by using different methods of concentration variation as described in Sec. 2. (temperature variation and variation of dilution flow). Since these experiments gave identical results, problems with the permeation sources at higher temperatures do not seem to occur and therefore cannot be the reason for the observed anomalous behaviour.

Possible reasons for the nonexponential decrease of reactant ions in the cases where cluster products were observed may include: (1) electric field induced collisional dissociation (ECD) of cluster ions behind the inlet orifice to the mass spectrometer, (2) reactions of formic or acetic acid dimers, and (3) thermal decomposition of cluster ions in the flow reactor.

When ions enter the quadrupole mass spectrometer through the inlet orifice, they are accelerated towards the quadrupole lens by an attractive potential difference between the sampling electrode and the quadrupole lens. In this expanding gas jet energetic collisions between neutral gas molecules and accelerated ions may happen, leading to fragmentation of cluster ions. In order to investigate the possibility whether ECD of product cluster ions may be a reason for the observed nonexponential kinetic behaviour the potential difference between the sampling electrode and the quadrupole lens was varied from the normally used value of 18–0 V. ECD is expected to decrease with decreasing potential difference between the sampling electrode and the quadrupole lens. These experiments showed that ECD can affect cluster ions, but that the effect of ECD is much too small for the present experimental conditions to explain the observed nonexponential behaviour.

Table 2
Ion-molecule reactions of formic acid with negative ions (p = 3 hPa, T = 293 ± 3 K)

Reaction	k_{meas}[a]	k_{coll}[b]
$OH^- + HCOOH \rightarrow HCOO^- + H_2O$	10 (±30%)	23
$O_2^- + HCOOH + M \rightarrow O_2^-HCOOH + M$	10 (±25%)[c]	19
$O_3^- + HCOOH \rightarrow HCOO^- + O_2 + OH$	11 (±25%)	17
$CO_4^- + HCOOH \rightarrow O_2^-HCOOH + CO_2$	9.3 (±30%)	15
$CO_3^- + HCOOH \rightarrow HCOO^- + CO_2 + OH$	7.4 (±25%)	16
$CO_3^-(H_2O) + HCOOH \rightarrow HCOO^- + CO_2 + OH + H_2O$	7.1 (±25%)[d]	16
$HCO_3^-(H_2O) + HCOOH \rightarrow HCO_3^-HCOOH + H_2O$	6.6 (±30%)[e]	16
$NO_3^- + HCOOH + M \rightarrow NO_3^-HCOOH + M$	4.5 (±25%)[c]	16
$NO_3^-(H_2O) + HCOOH \rightarrow NO_3^-HCOOH + H_2O$	17 (±25%)[f]	16
$NO_2^- + HCOOH + M \rightarrow NO_2^-HCOOH + M$	4.0 (±25%)[c]	17

[a]Measured reaction rate coefficient; all rate coefficients are reported in units of 10^{-10} cm^3 molecule^{-1} s^{-1}.
[b]Calculated collision rate coefficient (10^{-10} cm^3 molecule^{-1} s^{-1}); collision rate coefficients are calculated according to the theory of Su and Chesnavich [26].
[c]Effective binary reaction rate coefficient at 3 hPa synthetic air.
[d]Effective rate coefficient for hydrate composition $CO_3^-(H_2O)_n$: 50% $n = 1$, 50% $n = 2$.
[e]Effective rate coefficient for hydrate composition $HCO_3^-(H_2O)_n$: 26% $n = 1$, 74% $n = 2$.
[f]Effective rate coefficient for hydrate composition $NO_3^-(H_2O)_n$: 83% $n = 1$, 17% $n = 2$.

The equilibrium concentrations of formic and acetic acid dimers have already been estimated in Sec. 2. Equilibrium dimer concentrations in the flow reactor are very small and should not affect the reactions studied here. However, it may be possible that off-equilibrium conditions with significant concentrations of dimers persist over an appreciable part of the length of the flow reactor. If acid concentrations are increased the concentration of dimers should also increase. The decrease of reactant ions was found to be slower at higher acid concentrations. Thus, if dimer reactions were responsible for the observed nonexponential behaviour, the observations indicate that the reactivity of dimers should be less than the reactivity of monomers.

If so, a decrease in the acid concentration should therefore result in a faster, more monomerlike, reaction. The influence of dimers can also be decreased by using higher pressures and longer reaction times. At higher pressure a new equilibrium between monomers and dimers should be attained faster because of the higher amount of collisions. At longer reaction times the relative contribution of equilibration time should be less.

Fig 3 shows the measured abundances of CO_3^- and $CO_3^-(H_2O)_{0,1,2}$ both at 3 and 9 hPa plotted versus the product of acetic acid concentration and reaction time ($t_R \times [CH_3COOH]$). Reaction times were 10.5 ms for the 3 hPa and 32 ms for the 9 hPa experiments. Since acetic acid concentrations are lower, the reaction time is longer, and the pressure is higher; a faster reaction would be expected for the 9 hPa measurements if

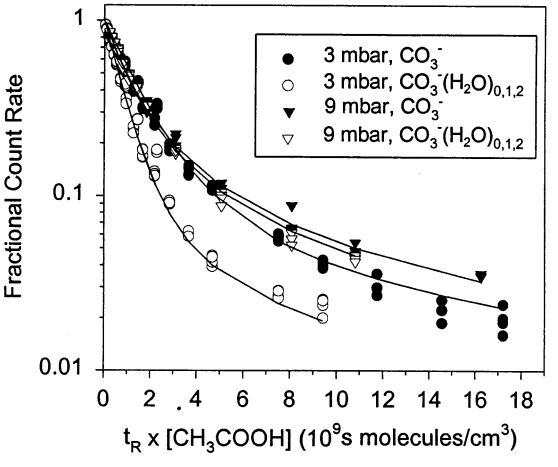

Fig. 3. Decrease of CO_3^- and $CO_3^-(H_2O)_{0,1,2}$ vs the product of reaction time and acetic acid concentration. Reaction times are 10.5 and 32 ms for 3 and 9 hPa flow reactor pressure ($N_2 + O_2$), respectively. The $CO_3^-(H_2O)_n$ hydrate distribution was 35%, 60%, and 5% for $n = 0$, 1, and 2 for the 3 hPa experiment, and 15%, 70%, and 15% for the 9 hPa experiment.

Table 3
Ion-molecule reactions of acetic acid with negative ions (p = 3 hPa, T = 293 ± 3 K)

Reaction		Yield (%)	k_{meas}[a]	k_{coll}[b]
CO_3^- + CH_3COOH	→ CH_3COO^- + CO_2 + OH	33	7.5 (±40%)	18
	$\xrightarrow{M}$ $CO_3^-CH_3COOH$	67[c]		
$CO_3^-(H_2O)$ + CH_3COOH	→ CH_3COO^- + CO_2 + OH + H_2O	33	17 (±30%)[d]	17
	→ $CO_3^-CH_3COOH$ + H_2O	67		
NO_3^- + CH_3COOH + M	→ $NO_3^-CH_3COOH$ + M	100	8.0 (±40%)[e]	18
$NO_3^-(H_2O)$ + CH_3COOH	→ $NO_3^-CH_3COOH$ + H_2O	100	17 (±40%)[f]	17
NO_2^- + CH_3COOH + M	→ $NO_2^-CH_3COOH$ + M	100	7.9 (±50%)[e]	20
$NO_2^-(H_2O)$ + CH_3COOH	→ $NO_2^-CH_3COOH$ + H_2O	100	18 (±50%)[g]	18

[a]Measured reaction rate coefficient; all rate coefficients are reported in units of 10^{-10} cm^3 $molecule^-$ s^-.
[b]Calculated collision rate coefficient (10^{-10} cm^3 $molecule^-$ s^-); collision rate coefficients are calculated according to the theory of Su and Chesnavich [26].
[c]Effective yield at 3 hPa synthetic air.
[d]Effective rate coefficient for hydrate composition $CO_3^-(H_2O)_n$: 92% n = 1, 8% n = 2.
[e]Effective binary reaction rate coefficient at 3 hPa synthetic air.
[f]Effective rate coefficient for hydrate composition $NO_3^-(H_2O)_n$: 85% n = 1, 15% n = 2.
[g]Effective rate coefficient for hydrate composition $NO_2^-(H_2O)_n$: 90% n = 1, 10% n = 2.

dimer reactions played a significant role. This was clearly not observed. For bare CO_3^- ions the two experiments at 3 and 9 hPa gave essentially identical results. In the case of hydrated CO_3^- a much stronger curvature starting at lower $t_R \times [CH_3COOH]$ can be observed at 9 hPa as compared to 3 hPa. These observations are not consistent with the assumption of dimer reactions as described above.

They are, however, consistent with the assumption of a backreaction being caused by the ultimate thermal decomposition of the $CO_3^-CH_3COOH$ cluster ion [reaction (6)]:

$$CO_3^- + CH_3COOH \rightarrow CH_3COO^- + CO_2 + OH \quad (2)$$

$$\xrightarrow{M} CO_3^-CH_3COOH \quad (3)$$

$$CO_3^-H_2O + CH_3COOH \rightarrow CH_3COO^- + H_2O + CO_2 + OH \quad (4)$$

$$\rightarrow CO_3^-CH_3COOH + H_2O \quad (5)$$

$$CO_3^-CH_3COOH \xrightarrow{M} CO_3^- + CH_3COOH \quad (6)$$

The identical behaviour of bare CO_3^- at 3 and 9 hPa and the different behaviour of hydrated CO_3^- can be understood if the cluster forming and breaking reactions (3) and (6) for bare CO_3^- have a similar pressure dependence. For hydrated CO_3^-, however, the cluster forming reaction (5) is a pressure independent exchange reaction, while the backreaction (6) increases with increasing pressure (increasing concentration of inert collision partners). The pressure dependence is thus balanced in the case of the opposing reactions (3) and (6) of bare CO_3^-, but not in the case of the opposing reactions (5) and (6) of hydrated CO_3^-.

At 9 hPa bare CO_3^- and hydrated CO_3^- show the same decay curves. Since the reaction of hydrated CO_3^- with acetic acid is a fast reaction occurring at the collision rate this indicates that the reaction of bare CO_3^- with acetic acid also is close to the collision rate and must therefore be at or close to its high pressure limit. Therefore also backreaction (6) must be close to the high pressure limit.

The relative contributions of the proton abstraction channels [reactions (2) and (4)] and the clustering channels [reactions (3) and (5)] for the bare and the hydrated case were determined by fitting the reaction kinetics of reactions (2)–(6) to the measured product ion distributions. The results are summarised in Table 3. For hydrated CO_3^- the branching ratio k_4/k_5 did not change between the 3 and 9 hPa experiments. For bare CO_3^-, the relative contribution of the addition channel

(3) seems to increase at higher pressures, which may be understood in terms of an increasing number of stabilising collisions at higher pressures [reaction (3)].

The lines in Fig. 3 are calculations using the reaction rate coefficients given in Table 3. The relative abundance of the hydrates $CO_3^-(H_2O)_n$ were 35%, 60%, and 5% for $n = 0$, 1, and 2, respectively, for the 3 hPa experiment, and 15%, 70%, and 15% for the 9 hPa experiment. For the backreaction (6) decomposition frequencies $k_6 = 50$ and 110 s^{-1} were used for the 3 and 9 hPa experiments, respectively.

It is possible that a second decomposition channel of $CO_3^-CH_3COOH$, associated with an intraclusteral proton transfer leading to CH_3COO^-, may play a role

$$CO_3^-CH_3COOH + M \rightarrow CH_3COO^- + CO_2 + OH + M \quad (7)$$

The yields in Table 3 are given assuming $k_7 = 0$. However, good agreement between the measured data and calculated values could also be obtained if it was assumed that all proton abstraction products were produced by reaction (7) only, i.e. $k_2 = k_4 = 0$. A possible contribution of reaction (7) to the formation of CH_3COO^- is therefore difficult to quantify.

The dissociation of the $CO_3^-CH_3COOH$ cluster ion was investigated with a triple quadrupole mass spectrometer [27]. Mass selected $CO_3^-CH_3COOH$ ions (mass: 120 amu) were directed to collide with an argon atom gas target at a collision energy of 35 eV. The only dissociation product observed was CO_3^- (mass: 60 amu) [Fig. 4(a)]. As one may expect, the collision induced dissociation of $CH_3COO^-CH_3COOH$ (mass: 119 amu) produced CH_3COO^- (mass: 59 amu) as the only dissociation product [Fig. 4(b)]. Thus at collision energies exceeding thermal energies $CO_3^-CH_3COOH$ only dissociates to CO_3^- and

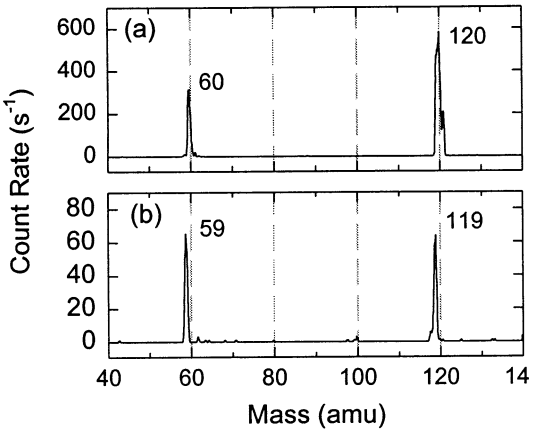

Fig. 4. Collision induced dissociation spectra of (a) $CO_3^-CH_3COOH$ and (b) $CH_3COO^-CH_3COOH$ with a triple quadrupole mass spectrometer (Ar gas target, collision energy 35 eV).

CH_3COOH. This result, however, cannot exclude the possibility that at lower (thermal) collision energies CH_3COO^- dissociation products may be formed [reaction (7)] in addition to CO_3^-.

The other cluster forming reactions with formic and acetic acids were also analysed in terms of backreactions. The results are compiled in Tables 2 and 3. From the ratios of the reaction rate coefficients for the forward and the backreactions equilibrium constants were obtained. The equilibrium constants are summarised in Table 4. Table 4 also gives the free energy changes for T = 293 K, ΔG^0_{293}, calculated from the equilibrium constants using the relation $\Delta G^0_{293} = -RT \ln (K_{eq})$.

5. Application for atmospheric measurements by IMRMS

The ion-molecule reactions of formic and acetic acids with negative ions described previously offer

Table 4
Equilibrium constants for selected cluster forming reactions (T = 293 ± 3 K)

Reaction	K_{eq} (atm^-)	ΔG^0_{293} (kcal mol^-)
$NO_3^- + HCOOH + M \leftrightarrow NO_3^-HCOOH + M$	3.2×10^8 (±50%)	−11.4 (±0.2)
$CO_3^- + CH_3COOH + M \leftrightarrow CO_3^-CH_3COOH + M$	2.6×10^8 (±50%)	−11.3 (±0.2)
$NO_3^- + CH_3COOH + M \leftrightarrow NO_3^-CH_3COOH + M$	5.7×10^8 (±50%)	−11.8 (±0.2)
$NO_2^- + CH_3COOH + M \leftrightarrow NO_2^-CH_3COOH + M$	1.2×10^9 (±50%)	−12.2 (±0.2)

the possibility for sensitive in situ and real-time measurements of atmospheric concentrations of formic and acetic acids. Useful reactions for atmospheric measurements of HCOOH and CH_3COOH are reactions with bare and hydrated CO_3^- or NO_3^- ions. These ions have previously been used for the measurement of acidic gases like HNO_3, HCN, HF, and H_2SO_4 and other gases [28–32].

If backreactions can be neglected the concentration of an acid (HA) can be obtained from the reaction kinetics using the measured ratio of product and reactant ions, R, the reaction rate coefficient, k_{HA}, for the reaction of the acid HA with the reactant ions, and the reaction time, t_R [27, 33]:

$$[HA] = \frac{1}{k_{HA} t_R} \ln(1 + R) \quad (8)$$

For $R = 10^{-4}$, $t_r = 50$ ms, and a flow reactor pressure of 40 hPa, a theoretical detection limit of a few ppt with a time resolution of a few seconds can be obtained for ambient HCOOH and CH_3COOH.

For many of the ion molecule reactions investigated in this work, relatively strong backreactions were observed in cases where cluster ions were formed. If the backreaction is fast enough compared to the total reaction time, a steady state for the reactant ions (X^-) and the product cluster ions (X^-HA) establishes. In this case the acid concentration [HA] can be inferred from the steady state by [34]:

$$[HA] = K_{eq}^{-1} \frac{[X^-HA]}{[X^-]} \quad (9)$$

The reaction of CO_3^- or $CO_3^-(H_2O)_n$ with acetic acid is a particularly interesting example, since it offers the possibility of inferring acetic acid concentrations via the proton abstraction reaction (4) using Eq. (8) and via the cluster forming reaction (5) using Eq. (9). At a flow reactor pressure of 9 hPa a decomposition rate constant for the $CO_3^-CH_3COOH$ cluster $k_6 = 110\ s^{-1}$ was inferred from the measurements, leading to a $CO_3^-CH_3COOH$ lifetime of 9 ms. Compared to the total residence time of 32 ms, this is short enough so that a steady state for the formation of $CO_3^-CH_3COOH$ via reaction (5) and the destruction of $CO_3^-CH_3COOH$ via the thermal decomposition reaction (6) can be established.

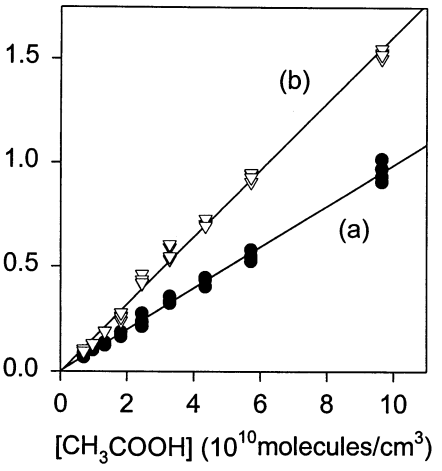

Fig. 5. Linear dependence of (a) $[CO_3^-CH_3COOH]/[CO_3^-]$ and (b) $\ln(1 + [CH_3COO^-]/[CO_3^-])$ on the concentration of acetic acid (measured at a flow reactor pressure of 9 hPa and a reaction time of 32 ms). The correlation coefficients are $r^2 > 0.99$ for both curves.

Fig. 5 shows the measured quantities $[CO_3^-CH_3COOH]/[CO_3^-]$ and $\ln(1 + [CH_3COO^-]/[CO_3^-])$ plotted versus the acetic acid concentration. For small acetic acid concentrations both curves show a linear dependence on $[CH_3COOH]$. Since the $CO_3^-H_2O + CH_3COOH$ reaction has the two reaction paths (4) and (5), the equilibrium constant cannot be directly inferred from the slope of the $[CO_3^-CH_3COOH]/[CO_3^-]$ curve. However, the very good linear behaviour of both curves shows that both methods can be used for measurements of acetic acid.

First ground-level test measurements of atmospheric HCOOH and CH_3COOH concentrations were performed at the Max-Planck-Institut in Heidelberg in December 1997. A typical mass spectrum from atmospheric measurements is shown in Fig. 6. The measurements were performed at a flow reactor pressure of 40 hPa and an ion residence time of 50 ms. The dominant ions are the reactant ions $CO_3^-(H_2O)_n$ produced by the ion source (masses 60, 78, 96 amu). Mass peaks consistent with the characteristic product ions $HCOO^-$ (formic acid) and CH_3COO^- (acetic acid) are well visible. The spectrum also shows an ion

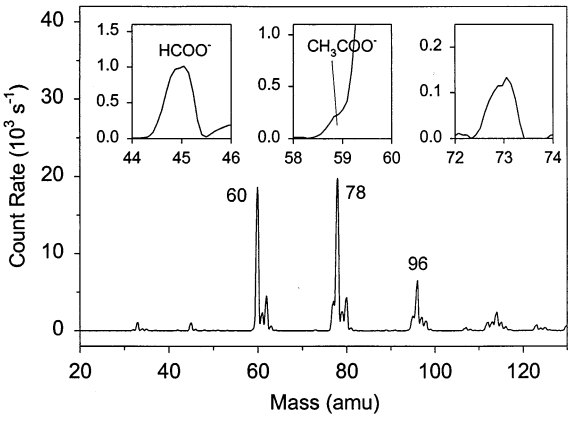

Fig. 6. Ion mass spectrum from atmospheric measurements. The mass spectrum was recorded on 9 December 1997, at the Max-Planck-Institut in Heidelberg. The insets show magnifications of the product ions from reactions of $CO_3^-(H_2O)_n$ with formic and acetic acids and the possible product of the reaction with propionic acid (mass 73 amu).

with a mass of 73 amu, which may be tentatively identified as $CH_3CH_2COO^-$, the possible product ion of the reaction of propionic acid (CH_3CH_2COOH) with CO_3^-.

Field calibrations were performed by the addition of known amounts of formic and acetic acids from permeation sources producing volume mixing ratios of up to 15 and 5 ppbv, respectively. Linear behaviour of the masses 45, 59, and 120 amu could be observed up to the maximum concentrations used during the calibration measurements. Atmospheric volume mixing ratios around 3 ppbv for formic acid and around 1 ppbv for acetic acid were obtained from these measurements.

As abovementioned ions with masses 45, 59, and 120 amu have previously been observed in ion mass spectra obtained from aircraft-borne measurements made by MPIK-Heidelberg in the upper troposphere and lower stratosphere. These measurements were performed using an atmospheric pressure flow reactor and a CO_3^- ion source [27]. From the ΔG^0_{293} value for the CO_3^- + CH_3COOH reaction obtained in the present work at 293 K, it can be estimated that at 255 K the equilibrium constant must be greater than 4.7×10^9 atm^{-1} [35]. This is almost 20 times higher than the room temperature value obtained in the present work. For a forward reaction rate coefficient $k_3 = k_5 = 11.4 \times 10^{-10}$ cm^3 $molecule^{-1}$ s^{-1} (k_3 being at the high pressure limit, i.e. collision rate, cf. Table 3) the cluster decomposition rate coefficient becomes $k_6 \leq 9.1$ s^{-1}, leading to a lifetime of more than 0.1 s for the $CO_3^-CH_3COOH$ cluster ion. During the aircraft measurements the ion residence time was about 10 ms. The effect of cluster decomposition was therefore very small for these measurements and the CO_3^- + CH_3COOH reaction system was far from equilibrium conditions. Under these conditions acetic acid concentrations can therefore be inferred from either CH_3COO^- or from $CO_3^-CH_3COOH$ product ions using the kinetics-based Eq. (8) and the appropriate reaction rate coefficients from Table 3 in both cases.

6. Summary and conclusions

Ion-molecule reactions of gaseous formic and acetic acids with several negative ion species have been investigated using a flow reactor. The latter was operated at a temperature of 293 ± 3 K and total gas pressures of 3 and 9 hPa. Reactant and product ions were measured by a quadrupole mass spectrometer. The reactions proceeded either via proton transfer, ligand switching (for hydrated reactant ions), or clustering. Measured rate coefficients for ligand switching of acetic acid all were close to the expected collision rate coefficients ($1.7–1.8 \times 10^9$ cm^3 $molecule^{-1}$ s^{-1}). Our present experiments provide a firm base for the quantitative detection of atmospheric gaseous formic and acetic acids by IMRMS. A first IMRMS-test measurement in ground-level air was carried out and potential product ions ($HCCO^-$, CH_3COO^-, $C_2H_5COO^-$) of formic, acetic, and eventually also propionic acids were indeed observed. Atmospheric volume mixing ratios determined from these first IMRMS-test measurements are 3 and 1 ppbv for formic and acetic acids, respectively. We plan future atmospheric IMRMS measurements which will also include unambiguous product ion identification by collision-induced dissociation investigations of mass selective product ions using a triple quadrupole mass spectrometer and an ion trap mass spectrometer.

Acknowledgements

Part of this work was funded by EU and BMBF. The stay of one of the authors (J.V.) at Heidelberg was partly funded by The Academy of Finland.

References

[1] R.W. Talbot, M.O. Andreae, H. Berresheim, D.J. Jacob, K.M. Beecher, J. Geophys. Res. 95 (1990) 16799.
[2] M.O. Andreae, R.W. Talbot, T.W. Andreae, R.C. Harriss, J. Geophys. Res. 93 (1988) 1616.
[3] K. Kawamura, S. Steinberg, I.R. Kaplan, Atmos. Environ. 30 (1996) 1035.
[4] H. Satsumabayashi, H. Kurita, Atmos. Environ. 24A (1990) 1443.
[5] S. Madronich, J.G. Calvert, J. Geophys. Res. 95 (1990) 5697.
[6] K. Kawamura, H. Kasukabe, O. Yasui, L.A. Barrie, Geophys. Res. Lett. 22 (1995) 1253.
[7] O. Horie, P. Neeb, S. Limbach, G.K. Moortgat, Geophys. Res. Lett. 21 (1994) 1523.
[8] P. Neeb, F. Sauer, O. Horie, G.K. Moortgat, Atmos. Environ. 31 (1997) 1417.
[9] G. Moortgat, B. Veyret, R. Lesclaux, J. Phys. Chem. 93 (1989) 2362.
[10] G. Moortgat, B. Veyret, R. Lesclaux, Chem. Phys. Lett. 160 (1989) 443.
[11] S. Madronich, R.B. Chatfield, J.G. Calvert, G.K. Moortgat, B. Veyret, R. Lesclaux, Geophys. Res. Lett. 17 (1990) 2361.
[12] W.C. Keene, R.W. Talbot, M.O. Andreae, K. Beecher, H. Berresheim, M. Castro, J.C. Farmer, J.N. Galloway, M.R. Hoffmann, S.-M. Li, J.R. Maben, J.W. Munger, R.B. Norton, A.A.P. Pszenny, H. Puxbaum, H. Westberg, W. Winiwarter, J. Geophys. Res. 94 (1989) 6457.
[13] E.G. Chapman, D.V. Kenny, K.M. Busness, J.M. Thorp, C.W. Spicer, Geophys. Res. Lett. 22 (1995) 405.
[14] W.C. Keene, J.N. Galloway, J.D. Holden Jr., J. Geophys. Res. 88 (1983) 5122.
[15] R.W. Talbot, B.W. Mosher, B.G. Heikes, D.J. Jacob, J.W. Munger, B.C. Daube, W.C. Keene, J.R. Maben, R.S. Artz, J. Geophys. Res. 100 (1995) 9335.
[16] O. Klemm, R.W. Talbot, D.R. Fitzgerald, K.I. Klemm, B.L. Lefer, J. Geophys. Res. (1994) 1687.
[17] W.C. Keene, J.N. Galloway, Atmos. Environ. 18 (1984) 2491.
[18] W.C. Keene, J.N. Galloway, Tellus 40B (1988) 322.
[19] O. Möhler, F. Arnold, J. Atmos. Chem. 13 (1991) 33.
[20] O. Möhler, T. Reiner, F. Arnold, J. Chem. Phys. 97 (1992) 8233.
[21] M.D. Taylor, J. Bruton, J. Am. Chem. Soc. 74 (1952) 4151.
[22] R. Büttner, G. Maurer, Ber. Bunsenges. Phys. Chem. 87 (1983) 877.
[23] D.K. Bohme, G.I. Mackay, S.D. Tanner, J. Am. Chem. Soc. 101 (1979) 3724.
[24] P.H. Wine, R.J. Astalos, R.L. Mauldin III, J. Phys. Chem. 89 (1985) 2620.
[25] S.G. Lias, J.E. Bartmess, J.F. Liebmann, J.L. Holmes, R.D. Levin, W.G. Mallard, J. Phys. Chem. Ref. Data 17 (1988) Suppl. 1.
[26] T. Su, W.J. Chesnavich, J. Phys. Chem. 76 (1982) 5183.
[27] O. Möhler, T. Reiner, F. Arnold, Rev. Sci. Instrum. 64 (1993) 1199.
[28] F. Eisele, D. Tanner, J. Geophys. Res. 98 (1993) 9001.
[29] H. Fischer, A.E. Waibel, M. Welling, F.G. Wienhold, T. Zenker, P.J. Crutzen, F. Arnold, V. Bürger, J. Schneider, A. Bregman, J. Lelieveld, P.C. Siegmund, J. Geophys. Res. 102 (1997) 23559.
[30] O. Möhler, F. Arnold, Geophys. Res. Lett. 19 (1992) 1763.
[31] J. Schneider, V. Bürger, F. Arnold, J. Geophys. Res. 102 (1997) 25501.
[32] F. Arnold, V. Bürger, B. Droste-Franke, F. Grimm, A. Krieger, J. Schneider, T. Stilp, Geophys. Res. Lett. 24 (1997) 3017.
[33] F. Arnold, G. Hauck, Nature 315 (1985) 307.
[34] L.G. Huey, E.R. Lovejoy, Int. J. Mass Spectrom. Ion Processes 155 (1996) 133.
[35] To exactly quantify the temperature dependence of the equilibrium constant, K_{eq}(T),ΔH^0 and ΔS^0 need to be known. Since $K_{eq} = \exp[-\Delta G^0/(RT)]$ and $\Delta G^0 = \Delta H^0 - T\Delta S^0$ the temperature dependence of K_{eq} is determined by the factor $\exp[-\Delta H^0/(RT)]$. Since the signs of the three quantities ΔG^0, ΔH^0, and ΔS^0 are negative, $|\Delta G^0| < |\Delta H^0|$ follows. Using $K_{eq}(T) = \exp[-\Delta G^0_{293}/(RT)]$ with a constant ΔG^0_{293} instead of the correct $K_{eq}(T) = \exp[-\Delta H^0/(RT)]\ \exp[-\Delta S^0/R]$ therefore underestimates the temperature dependence of K_{eq} and leads to an underestimation of K_{eq} at temperatures below 293 K and to an overestimation at temperatures above 293 K.